Effects of trailing edge shape on vortex formation by pitching panels of small aspect ratio

Arman Hemmati, Tyler Van Buren, and Alexander J. Smits

Phys. Rev. Fluids **4**, 033101 — Published 4 March 2019

DOI: 10.1103/PhysRevFluids.4.033101

Effects of trailing edge shape on vortex formation by pitching panels of small aspect ratio

Arman Hemmati,[1, 2, a)] Tyler Van Buren,[2] and Alexander J. Smits[2]

[1)] *Department of Mechanical Engineering, University of Alberta, Edmonton, AB, Canada T6G 1H9*

[2)] *Department of Mechanical and Aerospace Engineering, Princeton University, Princeton, NJ, USA 08544*

The effects of trailing edge shape on the vortex dynamics and surface pressure distributions on pitching foils are examined using direct numerical simulation. Results are presented for a Reynolds number of 10,000 and a Strouhal number of 0.5, which corresponds to the Strouhal number for maximum efficiency as found by experiment[1]. For the trailing edge shapes studied here (square, convex, and concave), the maximum instantaneous thrust occurs at the moment when the vortex detaches from the trailing edge. At the same time, the surface pressure gradients across the panel surfaces increase, while viscous forces drop. The leading edge vortices are seen to merge with the side edge shear layers, and as they wrap around the trailing edge the thrust generation is depressed just prior to the instance of maximum thrust. This process, combined with momentum transfer associated with switching the direction of pitching, produces irregular variations in the thrust and side forces. Compared to the square panel, the wake of a concave trailing edge panel exhibits strong three-dimensional effects on its side edges leading to slower wake contraction, smoother vortex bending, and lower thrust. In contrast, the convex trailing edge panel allows detaching structures to grow longer prior to their detachment, resulting in bent structures formed closer to the trailing edge, which leads to faster wake contraction and higher thrust. Skeleton models of the wakes help explain their underlying structure.

Keywords: Pitching Panel, Wake Dynamics, Swimming, Trailing Edge, Direct Numerical Simulation, Immersed Boundary Method

[a)] Electronic mail: arman.hemmati@ualberta.ca

I. INTRODUCTION:

Understanding the mechanics of swimming may inspire the design of propulsors for underwater vehicles that match or surpass those of biological species[2,3]. With this aim in mind, many previous studies have examined the performance and wake structures produced by simple foils undergoing oscillating motions[4–7]. The performance is usually described in terms of thrust coefficient, C_t, a power coefficient C_P, and a Froude efficiency η, where

$$\eta = \frac{C_t}{C_P}, \qquad C_t = \frac{F_x}{\frac{1}{2}\rho U_\infty^2 S}, \qquad C_P = \frac{P}{\frac{1}{2}\rho U_\infty^3 S}.$$

Here F_x is thrust, P is power, ρ is the density of the fluid, U_∞ is the freestream velocity, and S is the planform area of the foil (for a rectangular foil, $S = cs$ where c is the chord length and s is the span). It is widely observed that the thrust and power coefficients increase monotonically with Strouhal number, while the efficiency typically exhibits a peak at a Strouhal number in the range of 0.2 to 0.4, which corresponds well to the range of Strouhal numbers observed for fish swimming in cruise[8]. The Strouhal number is defined by $St = 2f_p a/U_\infty$, where a is the amplitude of the trailing edge motion, and f_p is the frequency of actuation in Hz.

For low aspect ratio rectangular pitching foils, the complexities of the highly three-dimensional wake structure have been well documented[6,9,10]. Broadly speaking, the near field is marked by the compression of the wake in the plane of the panel, and a concomitant expansion in the orthogonal direction. The particular downstream evolution depends strongly on the Strouhal number. At low Strouhal numbers (0.2 to 0.3) the wake in the plane normal to the panel typically appears as a reverse von Kármán street, with two horseshoe vortices shed per pitching cycle that interact with neighboring structures to form a three-dimensional chain of vortex loops. With increasing Strouhal number, the wake typically bifurcates into two oblique trains of vortex structures, although many other possibilities exist[6].

With respect to the wake structure, Green et al.[11,12] investigated the three-dimensional wakes of rigid pitching panels with a trapezoidal planform, chosen to model idealized truncate caudal fins. A classic reverse von Kármán vortex street pattern was observed along the mid-span of the near wake, but the vortices realigned and exhibited strong interactions near the spanwise edges of the wake. At higher Strouhal numbers, the complexity of the wake

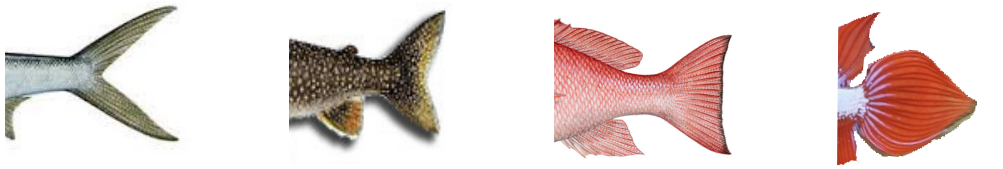

FIG. 1: Different types of fish tail[1,13].

increased downstream of the trailing edge as the spanwise vortices spread transversely and lost coherence as the wake split.

Such studies can be useful in understanding animal swimming, particularly for animals that use their caudal fin or fluke as the major source of thrust. Rectangular foils, however, are an extreme simplification of what is seen in biology where there exists a wide variety of fish tail shapes[13] (Figure 1). It is also well known that the planform shape impacts the propulsive performance. For example, Chopra[14] examined numerically the impact of pitching and heaving amplitudes on the performance of different lunate tails (characteristic of cetaceans as well as fast swimming fish), and found that fin shape significantly affects the conditions for maximum efficiency. Karpouzian et al.[15] similarly found for lunate tails that sweep has a major effect on the propulsive performance. Liu and Dong[16] studied the hydrodynamic performance and wake patterns generated by fish caudal fins in flapping motion, and found that the lunate shape model (high aspect-ratio) always generated a larger thrust compared to other models. They also found that the large aspect ratio fins (tuna and shark) have a higher efficiency when the Strouhal number is in the range of steady swimming ($0.2 < St < 0.4$), while the lower aspect ratio caudal fins (catfish and trout) are more efficient when $St > 0.4$.

More recently, Van Buren et al.[1] studied the effects of the trailing edge shape on the propulsive performance of pitching foils. They categorized different trailing edge shapes based on the trailing edge angle, ϕ (see Figure 2). The foils maintained a constant area, but ϕ was systematically varied from 45° to 135°. Their experiments indicated that convex trailing edges ($\phi > 90°$) have better propulsive performance (thrust and efficiency) than rectangular ($\phi = 90°$) or concave shapes ($\phi < 90°$), and trends in performance could be linked to changes in the wake structure. Due to the limitations of their experiment it was not possible to gain insight on how the wake structure, thrust production and instantaneous surface pressure

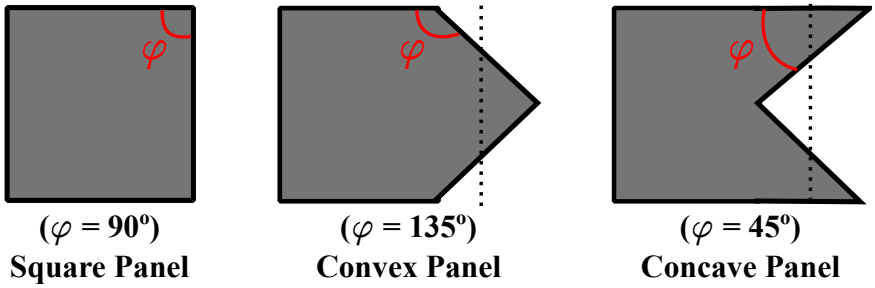

FIG. 2: Foil planforms showing variations in trailing edge shape. Van Buren at al.[1] studied cases where $45° \leq \phi \leq 135°$ in intervals of 15°.

distributions were related. However, the pressure measurements by Green and Smits[17] along the midspan of a low aspect ratio rectangular panel showed that the maximum and minimum pressures were associated with the extrema of the panel acceleration. When the panel motion reached its maximum amplitude, a positive streamwise pressure gradient existed along the surface that was about to advance, which is in contrast to steady flow at the same angle of incidence where a negative pressure gradient is seen.

In a related study using a robotic lamprey, Leftwich et al.[18] found that the amplitude of the phase-averaged surface pressure distribution along the centerline of the body increased in the posterior direction, indicating that the thrust is produced mainly at the tail. Also, the phase relationship between the pressure signal and the vortex shedding from the tail showed a clear connection between the location of vortex structures and the fluctuations of the pressure signal. Similar observations were made by Hemmati et al.[19,20], who demonstrated that vortex shedding behind a normal thin flat plate is marked by an abrupt change in the surface pressure distribution.

Here, we expand on the experimental work by Van Buren et al.[1] on foils with different trailing edge shapes to gain additional insight on the vortex structure of the wake, its connection to the instantaneous pressure distribution on the foil, and its thrust performance. For simplicity, we will consider only three particular cases: the square trailing edge with $\phi = 90°$, the convex trailing edge with $\phi = 135°$, and the concave trailing edge with $\phi = 45°$ (see Figure 2). We examine their propulsive performance and wake structure using a new Immersed Boundary Method (IBM). The Reynolds number ($Re = U_\infty c/\nu$) was fixed at 10,000, high enough so that the effects of Reynolds number on performance are small[21]. The Strouhal number was fixed at 0.5, which corresponds to the Strouhal number for maximum

efficiency as found in the experiments by Van Buren et al.[1] at the same Reynolds number[1].

II. PROBLEM DESCRIPTION

The three-dimensional incompressible Navier-Stokes and continuity equations were solved directly using a new Immersed Boundary Method in OpenFOAM, as described by Şentürk et al.[22]. The second-order backward Euler method was used for temporal discretization, and central differences were used for spatial discretization. All variables were normalized by the panel chord (c) and the uniform inlet velocity (U_∞). More details on the numerical schemes and the base solver can be found in Senturk and Smits[21] and Brunner[23].

The computational domain, shown in Figure 3, was designed to best replicate conditions in the water tunnel experiment by Van Buren et al.[1]. A Cartesian coordinate system was used with the computational domain extending $25c$ in the flow x-direction and $5c$ in the spanwise y- and z-directions. The rigid panels were located $5c$ downstream of the inlet and

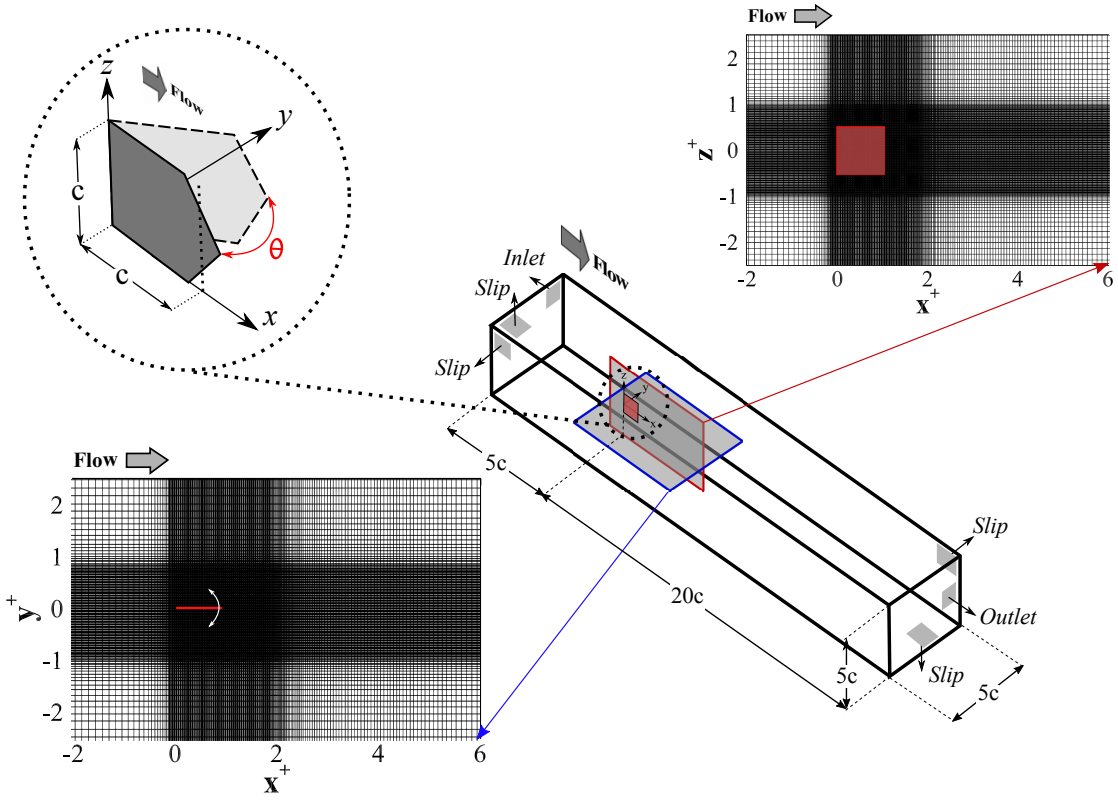

FIG. 3: Computational domain (not to scale), showing mesh distribution around the panel on the central $xy-$ and $xz-$planes.

2.5c from all side boundaries. The effect of domain size on results were investigated by Şentürk et al.[22]. The domain size was similar to that used by Taira and Colonius[24].

The panel was pitched about its leading edge, coinciding with the z-axis, and its motion was defined by

$$\theta(t) = \theta_0 \sin(2\pi f_p t), \tag{1}$$

where θ is the pitch angle (see top-right of Figure 3), and t is time. The maximum pitch angle (θ_0) was kept constant at 8°, and the Strouhal number was fixed at a value of 0.5. Three symmetric trailing edge shapes were used as shown in Figure 2, with square, convex and concave trailing edges defined by $\phi = 90°$, 135° and 45°, respectively. All three panels had the same area, and the same aspect ratio $AR = s/\bar{c} = 1.0$, where $\bar{c}$ is the average chord length.

At the inlet boundary, the flow was set to be uniform ($u = U_\infty, v = w = 0$) with no acceleration ($\partial p/\partial n = 0$), while at the outlet boundary the Neumann outflow condition was used ($\partial U/\partial n = \partial p/\partial n = 0$). The slip boundary condition ($\partial U/\partial \tau = 0$, $\mathbf{U} \cdot \mathbf{n} = 0$, and $\partial p/\partial n = 0$) was imposed on all side boundaries. The panel thickness was one spatial grid element, which constitutes a panel with zero-thickness[25].

Since the near wake flow is expected to be dominated by large scale structures that are the most significant contributors to the aerodynamics forces, a non-homogeneous spatial grid was used with higher grid resolution concentrated around the panel and in the immediate wake (see Figure 3). The non-linear dynamics of the large-scale structures can be accurately captured by discretizing the Navier-Stokes equations and letting the numerical discretization filter the unresolved scales. In order to study the effects of grid size, three different grids were used, where *Grid 1* had 1.13×10^6 elements, *Grid 2* had 3.24×10^6 elements and *Grid 3* had 9.82×10^6 elements. The temporal grid was adjusted such that the maximum CFL number for all three cases was less than 0.6. The comparison of the coefficients of thrust and side-force amongst the three cases shown in Figure 4 identified that *Grid 1* is insufficient, whereas the difference between *Grid 2* and *Grid 3* was 4% at $t^\star = 0.48$, where the differences between C_s values are the largest. *Grid 3* was used for all the results presented here. The normalized timestep was fixed at 5.0×10^{-4}. The convergence criterion was set as a pressure and velocity tolerance of 10^{-6} using a combined pressure-implicit split-operator (PISO) and semi-implicit method for pressure-linked equations (SIMPLE) algorithms referred to as

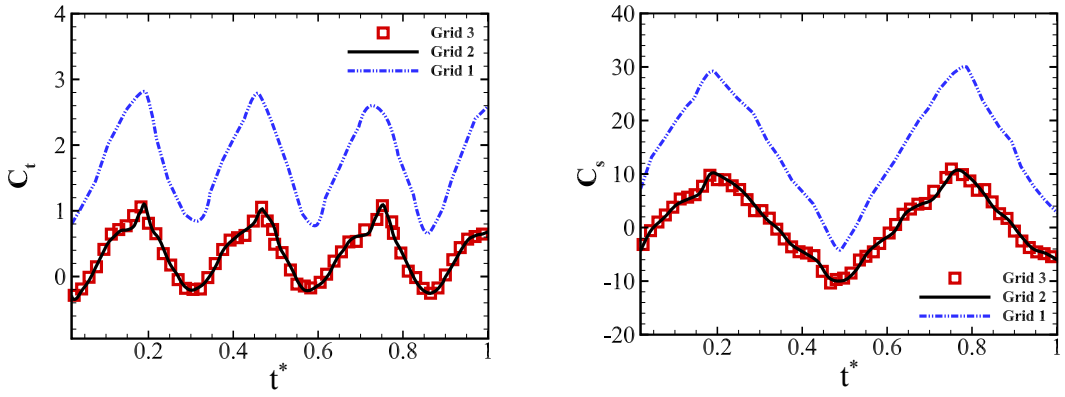

FIG. 4: Grid-independence study based on (left) coefficient of thrust, and (right) coefficient of side-force.

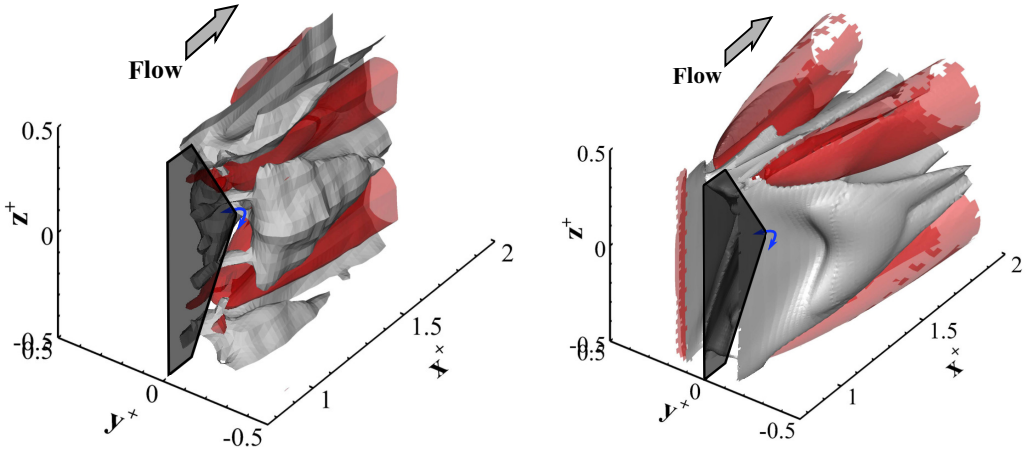

FIG. 5: Iso-surface of mean velocity magnitude ($\overline{u^\star} = 0.96$ - Gray, $= 1.03$ - Red) at $St = 0.2$. Left: experiments[1] at $Re = 6,000$. Right: simulations at $Re = 10,000$.

PIMPLE.

The results on the instantaneous wake structure may also be compared for the case of $St = 0.2$ with the PIV data of Van Buren et al.[1]. Figure 5 compares iso-surface of $\overline{u^\star}$ immediately behind the panel trailing edge between the current study and PIV measurements. The results show some differences, which are most likely due to the limited resolution of the PIV data, and the differences in Reynolds number. The overall wake structure, however, appears to be well-captured by the simulations.

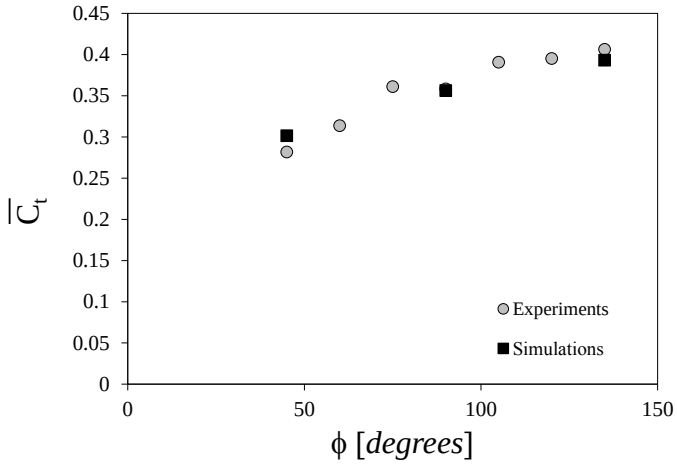

FIG. 6: Mean thrust coefficient ($\overline{C_t}$) at $St = 0.5$. Current results at $Re = 10,000$ compared with experiment at the same Reynolds number[1]. The trailing edge angle ϕ is defined in Figure 2.

III. THRUST RESULTS

Figure 6 shows the variation of time-averaged thrust coefficient, $\overline{C_t}$, with the trailing edge angle. The numerical results at $Re = 10,000$ are in good agreement with the experimental results at the same Strouhal number[1], where the experiment was performed at $Re = 6,000$ for the wake study and 10,000 for the performance data. We also see that the mean thrust is a strong function of the trailing edge angle, and that it increases by about 10% between $\phi = 45°$ and $\phi = 135°$. Van Buren et al.[1] found that the convex panel produced more thrust and a higher efficiency than the square panel, while the concave panel produced less thrust and a lower efficiency. By studying the wake formation process, and its connection to the instantaneous pressure distributions on the panel surfaces (which are directly related to the thrust generation), we hope to illuminate this dependence on trailing edge shape.

IV. EFFECT OF TRAILING EDGE SHAPE ON WAKE STRUCTURE

To give an overview of the effects of the trailing edge on the wake structure, we show in Figure 7 iso-surfaces of the λ_2 criteria in the xz-plane. Here, λ_2 is the second eigenvalue of the $S_{ik}S_{kj} + \Omega_{ik}\Omega_{kj}$ tensor with S_{ij} and Ω_{ij} being the strain-rate and rotation-rate tensors, respectively[26]. Figure 7 shows the wake structures from the top-view (xz-plane) for each

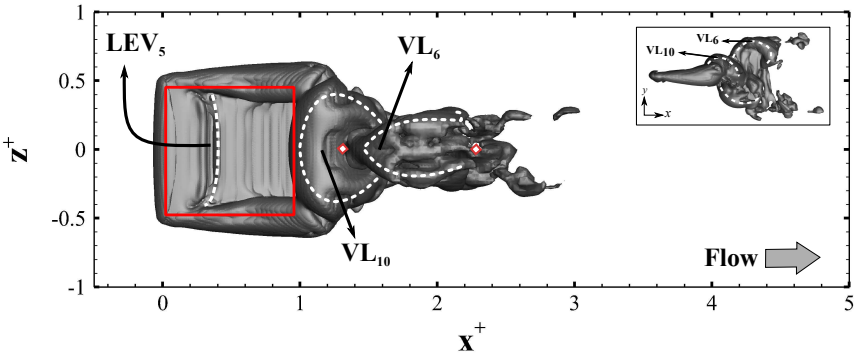

(a) Square Panel

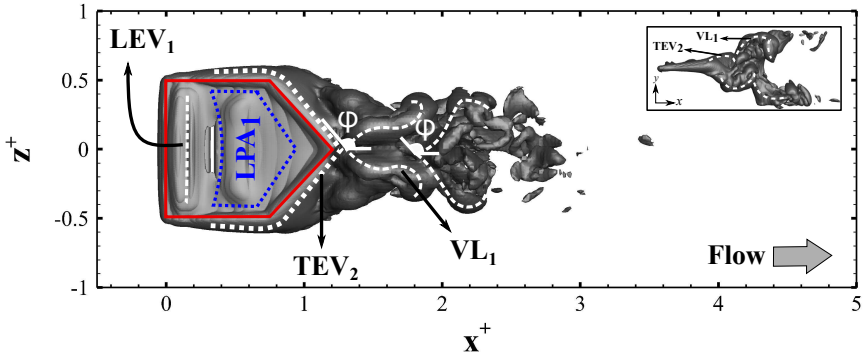

(b) Convex Panel

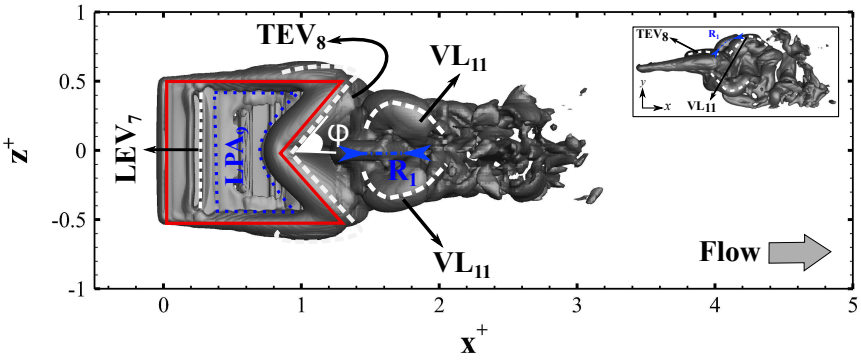

(c) Concave Panel

FIG. 7: The iso-surface of $\lambda_2 = -20$ for three panels, immediately prior to instance of maximum thrust. The inter-locked vortex loops are identified with dotted lines.

panel.

For the square panel (Figure 7a), the overall wake structure is similar to that observed by Buchholz and Smits[9] for a low aspect ratio rectangular panel with $St = 0.43$ at a lower Reynolds number. The initially circular shaped vortex loops change to ellipses farther down-

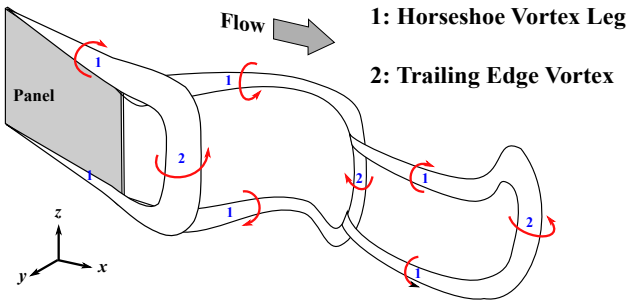

(a) Square trailing panel.

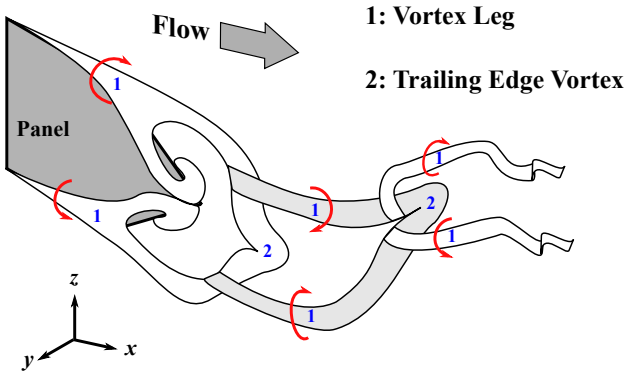

(b) Convex trailing panel

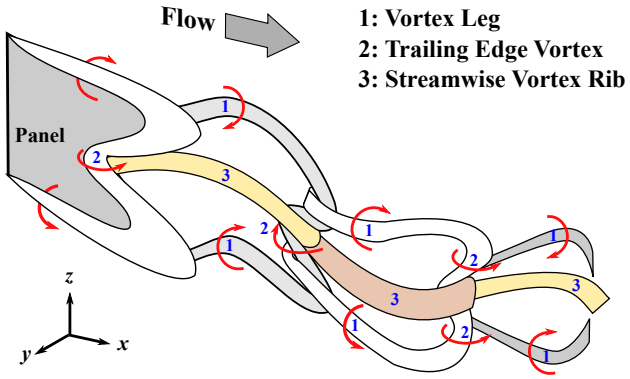

(c) Concave trailing panel

FIG. 8: Model vortex skeletons. Different shades of color indicate different directions of rotation.

stream in the wake due to the vortex interactions, which Buchholz and Smits[6] attributed to the opposite-sign vorticity interaction of streamwise vortex legs (VL) and trailing edge vortices (TEV). For $x^+ = x/\bar{c} > 3$, the wake becomes highly distorted and diffuse.

For the convex panel (Figure 7b), the linked vortex loops in the wake retain the imprint

of the trailing edge shape as they develop downstream. As in the case of the square panel, the streamwise vortex legs connect the TEV to the panel. However, the convex shape of the trailing edge causes a distortion that leads to the formation of an arc-shape structure downstream. The interactions among successive structures cause strong deformations, and eventually break down the initially linked (chain-like) vortex loops. It appears that the convex shape of the trailing edge, in particular the trailing tips, extend the panel surface farther into the wake, which allows additional growth before the trailing edge structures detach. The side-edge shear layers merge at the convex point of the trailing edge and form a single large structure. Moreover, the vortex loops remain connected at the point of separation from the panel downstream, and the structures tend to retain the shape of the trailing edge.

In contrast, the wake structure of the concave panel does not retain the shape of the trailing edge (Figure 7c). Streamwise vortex ribs (shown by the blue dotted lines) are formed at the interior corner of the trailing edge which distort the detached vortex loops, and so their initial shape is quickly distorted. This behavior is consistent with that seen by Van Buren et al.[1], although they found that the shape retention of the vortex structure depends not only on the Strouhal number, but also on the frequency and amplitude combinations for a given Strouhal number. That is, for the same Strouhal number, at lower frequencies the trailing edge vortex was found to retain its shape, while at higher frequencies the trailing edge vortex broke down quickly.

These observations on the wake structure are embodied in the vortex skeleton models shown in Figure 8. The circular arrows identify the direction and sign of vorticity for each structure. For the square panel, streamwise vortex legs connect consecutive structures in the wake, which eventually connect back to the panel. These vortex legs are entrained toward the panel centerline, leading to bent structures. The model tries to capture the narrowing of the wake in the plane of the panel and the splitting of the wake in the plane of pitching. This superficially resembles the model by Buchholz and Smits[10] for a low aspect ratio rectangular panel at $St = 0.43$, where the wake was also seen to split. Despite their initial interconnection, the TEVs (and their subsequent vortex loops) that are formed at the end of a pitching stroke separate from one another to form two separate vortex streets.

For the convex panel, the model shows how the orientation of the structures and their subsequent interaction is influenced by the trailing edge shape. The initially streamwise

vortex legs move down the trailing edge and lock at the tip of the TEV (vortex 2 in Figure 8b), which strongly distorts the structures further downstream. The degree of wake splitting is not as severe as that seen for the square panel. The detachment of TEVs from the convex panel occurs at the panel tip, which increases their opportunity for growth prior to detachment. This results in the formation of relatively larger structures at the time of their detachment, which is directly related to larger thrust generated by the convex panel compared to the square one.

For the concave panel, the model highlights the significance of the streamwise ribs (vortex 3 in Figure 8c) in connecting recently detached TEVs (vortex 2). The interaction of these structures with TEVs results in their mutual distortion. The vortex legs that were initially connected to the side-edge shear layers (labeled 1 in Figure 8c), lock consecutive structures at locations adjacent to those of streamwise ribs (vortex 3), which further intensifies the distortion of the vortex structures downstream. We will see that the effects of three-dimensionality associated with side-edge shear layers contributes to lowering the thrust produced by the concave panel[17].

To examine the connections between wake formation and the forces produced by each panel, we now consider the flow in the vicinity of each panel at some selected instances during the pitching cycle. We focus primarily on the convex panel because the results for the other two panels are broadly similar.

V. CONVEX PANEL WAKE AND FORCE PRODUCTION

To investigate the connection between the wake structure and the forces that are generated by the panel, the pitching motion will be split into two stages: the inward pitch and the outward pitch. During the inward pitch, the panel moves from the maximum magnitude of the pitch angle ($|\theta| = \theta_0$) to its neutral state ($\theta = 0$). Conversely, during the outward pitch the panel moves from the neutral state to $|\theta| = \theta_0$. The orientation where $\theta = +\theta_0$ is referred to as the high-pitch state, whereas the orientation where $\theta = -\theta_0$ is called the low-pitch state. The face of the panel with a normal in positive y-direction is referred to as the *left face*, and the one facing the negative y-direction is referred to as the *right face*. The vortex cores are identified using the λ_2 criterion.

For the convex panel, the variations of the instantaneous thrust and side force coefficients

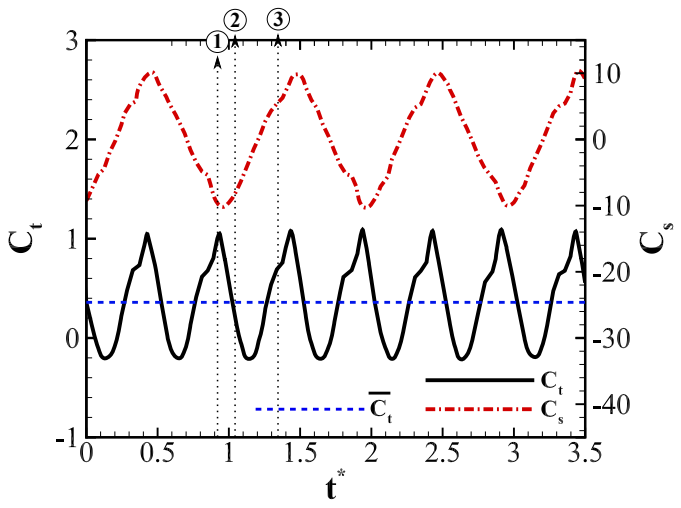

FIG. 9: Thrust (C_t) and side-force (C_s) coefficients for the convex panel ($\phi = 135°$). Instances 1 and 2 are selected to examine the wake prior to and after the instance of maximum thrust. Instance 3 is selected to evaluate the events coinciding with irregularities in force variations.

(C_s and C_t) over four pitching cycles are shown in Figure 9. The non-dimensional time is defined as $t^\star = tf_p$, so that at this Strouhal number (0.5) a full cycle is completed for $\Delta t^\star = 1$. As expected, the thrust oscillates at twice the frequency of the side-force fluctuations, and the instances of maximum thrust coincide with maximum and minimum side-forces, whereas the instances of minimum thrust correspond with the change of slope for the side-force. There are small irregularities in thrust that correspond to a similar behavior in side-force variations (see $t^\star = 0.33$, 0.83, 1.33 and so on), which are associated with specific vortex dynamics as discussed later in this section. Moreover, these irregularities are periodic with a frequency of $2f_p$, and they occur $\Delta t^\star = 0.11$ prior to the instance of maximum thrust and maximum/minimum side-force. Three instances (1, 2, and 3) are highlighted in Figure 9, corresponding to $t^\star = 0.91$, 1.02, and 1.32, respectively. These instances correspond to specific events leading to maximum thrust ($1 \rightarrow 2$), while instance 3 coincides with irregularities in thrust and side-force fluctuations. We now consider these instances in more detail.

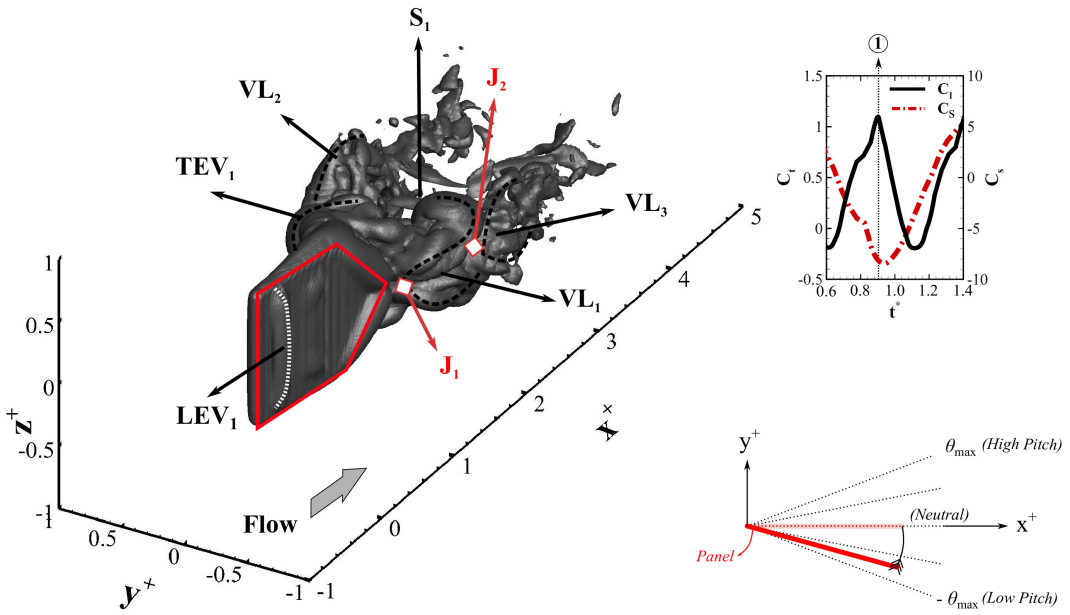

FIG. 10: Convex trailing edge panel at instance 1 ($t^\star = 0.91$). Left: isosurfaces of $\lambda_2 = -10$. Top right: variation of C_t and C_s. Bottom right: panel orientation.

A. Instance 1 ($t^\star = 0.91$)

Figure 10 shows the structures defined by the iso-surfaces of λ_2, together with the force fluctuations (top-right corner) at instance 1 ($t^\star = 0.91$). As shown on the bottom-right corner of Figure 10, the panel is in an inward pitching motion ($\theta \to 0$) with $\theta = -0.875\theta_0$. It has reversed its direction of pitching after reaching the low pitch state. We see a new leading edge vortex, identified as LEV_1, forming on the right face of the panel. A developing vortex loop VL_1 is formed by the transformation of a trailing edge vortex (TEV) that is still attached to the panel's trailing edge at point J_2, which connects to the farthest point of the trailing edge. Two previously detached vortex loops, VL_2 and VL_3, move downstream while remaining connected to the newly formed structures, TEV_1 and VL_3, respectively. For example, J_2 identifies the point of connection between VL_1 and VL_3. TEV_1 in Figure 10 identifies a developing trailing edge structure that remains connected to the panel shear layers that are formed on the panel upper and lower (side) edges. It seems likely, based on the vortex interaction and distortion, that a high strain-rate zone exists between the detaching Trailing Edge Vortex (TEV_1) and the panel surface, which leads to pressure variations on the corresponding surface. The surface pressure signatures are discussed in Section VIII.

We see that the wake appears to split into two streets around point S_1, and there are no major structures identifiable along the centerline of the wake downstream of S_1. Contours of vorticity components, not included for brevity, identify this as a point of transition from a large angle of wake expansion ($\approx 51°$) to a low angle ($\approx 10°$).

The thrust reaches its maximum local value (see top-right-corner of Figure 10) at the same time as VL_1 is on the verge of detachment from the panel. Moreover, this event coincides with the point of minimum side-force. It should be noted that the maximum thrust does not occur when the panel reaches its low-pitch state ($\theta = -\theta_0$), but shortly after the direction of oscillation changes from an outward pitching motion ($|\theta| \to \theta_0$) to an inward pitching motion ($\theta \to 0$). The corresponding pressure distributions on the panel surfaces are discussed in Section VIII.

B. Instance 2 ($t^\star = 1.02$)

Figure 11 shows the structures and force variations at instance 2 ($t^\star = 1.02$), which coincides with the panel approaching its neutral state with $\theta = -0.05\theta_0$ in an inward pitching motion ($\theta \to 0$). LEV_1 in Figure 11 has moved towards the trailing edge compared to where it was in Figure 10, and it is merging with the side-edge shear layers at $x^+ = x/c \approx 0.4$.

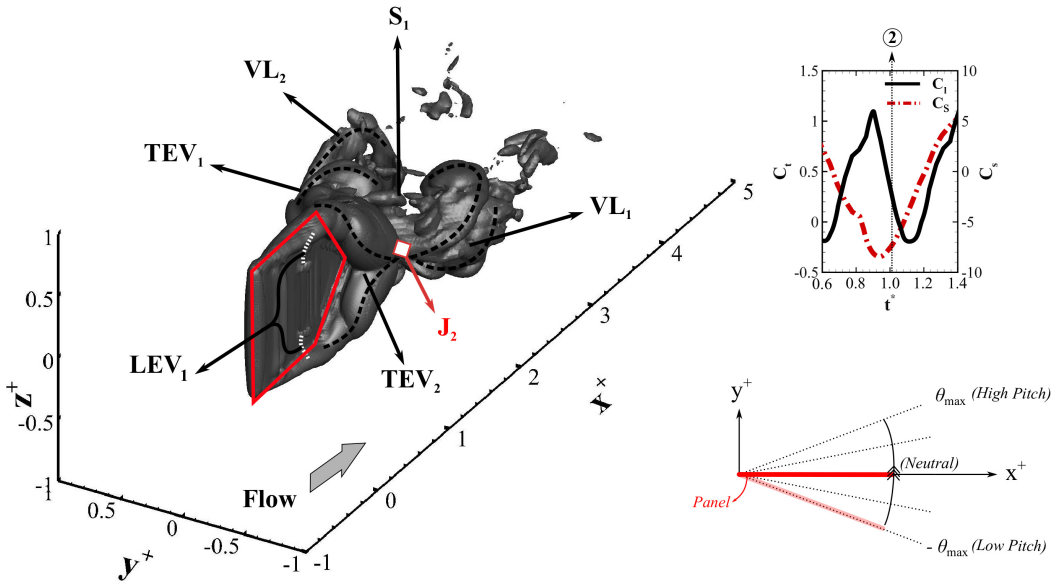

FIG. 11: Convex trailing edge panel at instance 2 ($t^\star = 1.02$). For symbols and notation see Figure 10.

This is followed by wrapping of side-edge shear layers around the trailing edge to feed the newly forming TEV_2. At this instance, VL_3 appears to have distorted to the point that it cannot be identified as a structure using the set λ_2 threshold. The newly detached structure, VL_1, is bent towards the wake centerline at $x^+ \approx 3$, while it remains connected to the newly forming TEV_2 at J_1 and continues to retain the shape of trailing edge. Although not fully visible, TEV_1 is expanding while remaining attached to the panel trailing edge. These wake events coincide with a change of slope for the thrust, while the side force is starting to increase after reaching its minimum local value.

Comparing the wake at instances 1 and 2 identifies the detachment of VL_1 (which itself is a detached TEV) from the panel as the main event coinciding with C_t approaching its maximum local value. At instance 1, VL_1 is still attached to the panel trailing edge at J_1, but at instance 2 it is fully detached from the panel with J_1 now acting as the connecting point between the detached structure (VL_1) and the newly forming structure (TEV_2). LEV_1 has broken down during this period and it has started merging with side-edge shear layers (see Figure 11). This process was followed by the initial formation of TEV_2 on the trailing edge of the panel. Also VL_1 at instance 2, compared to its shape at instance 1, is stretched while bending towards the wake centerline. However, VL_1 retains the shape of the training edge due to its connection with the newly forming TEV_2 at J_1.

C. Instance 3 ($t^\star = 1.32$)

The wake behavior at instance 3 ($t^\star = 1.32$) is shown in Figure 12. Some irregular reductions in thrust occur around this time, where the panel is approaching its high-pitch state ($\theta = +\theta_0$). The principal factor that leads to the local suppression of thrust may be that VL_4 stays connected to the panel for a longer distance before it detaches (not visible in Figure 12). This leads to the stretching of TEV_2 as it expands while connected to the side-edge shear layers. Moreover, it appears that structures that are attached to the panel (that is, TEV_2 and VL_4 - formerly TEV_1) are pulled along by the panel motion. The size of these structures, specially VL_4 (formerly TEV_1), is comparable to that of the panel itself, and this has significant implications in terms of momentum transfer. In addition, the previously formed structures appear to experience some stretching and distortion. For example, VL_1 appears to be highly bent, although it remains attached to other structures in the wake at

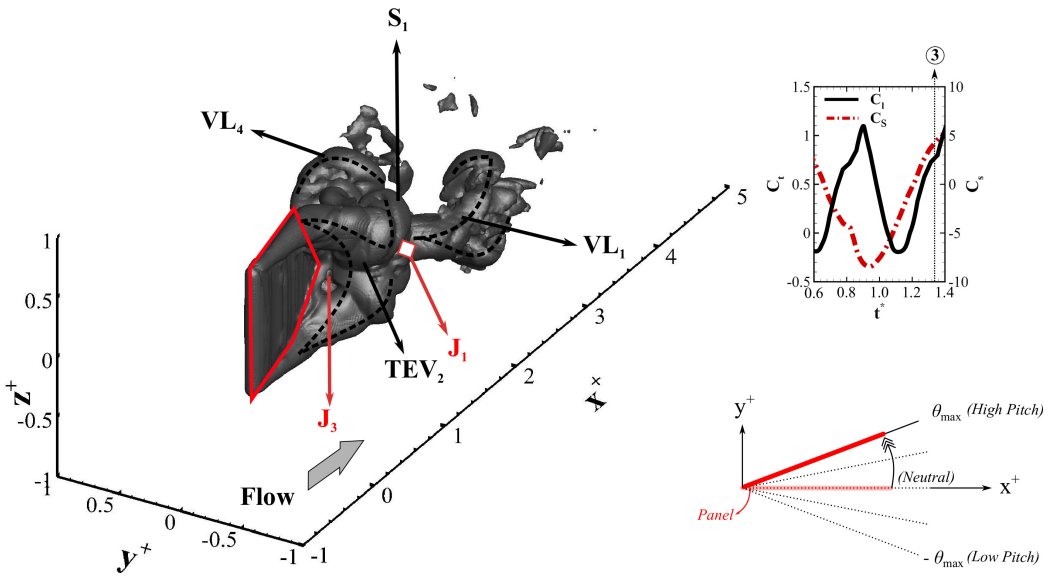

FIG. 12: Convex trailing edge panel at instance 3 ($t^\star = 1.32$). For symbols and notation see Figure 10.

J_1 by a secondary structure similar to a streamwise vortex leg. The wake remains split at S_1.

The local (in time) reduction in thrust coincides with a similar irregularity in the side-force. This occurs as the panel switches from an outward pitching motion ($|\theta| \to \theta_0$) to an inward pitching motion ($\theta \to 0$), implying that the behavior of C_t and C_s are tied to a significant change in momentum transfer associated with the switch in direction.

VI. SQUARE PANEL WAKE AND FORCE PRODUCTION

The instantaneous thrust and side-force variations for the square panel are shown in Figure 13 over three pitching cycles. The general behavior is very similar to that seen for the convex panel in Figure 9. The instances of maximum thrust coincide with the side-force local extrema at $t^\star = 0.44$ and 0.93 in the first period. We see local reductions in thrust, similar to those observed for the convex panel, at $t^\star = 0.33$ and 0.86, which correspond to simultaneous irregularities in the side-force. These events occur prior to instances of maximum thrust, just before the local maximum and minimum in C_s, and they are related to additional growth of the TEV before it detaches, as observed for the convex panel. Instance 4 ($t^\star = 0.93$) occurs around the time of maximum C_t, and instance 5 ($t^\star = 1.32$) occurs

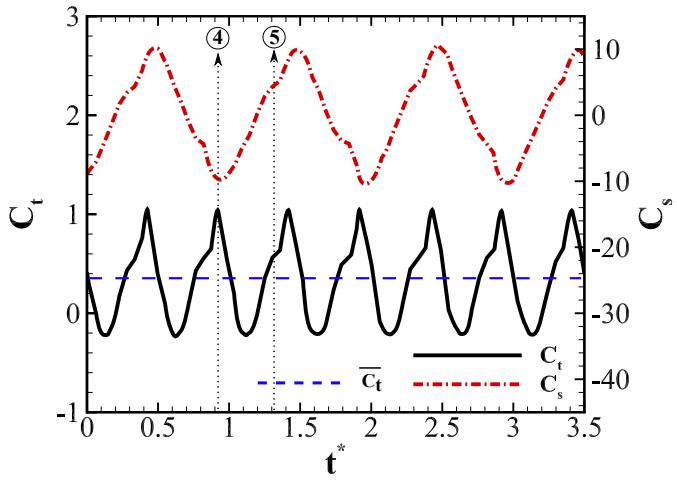

FIG. 13: Thrust (C_t) and side-force (C_s) coefficients for the square panel. Instance 4 ($t^\star = 0.93$) corresponds to the high-pitch panel orientations, while instance 5 ($t^\star = 1.32$) corresponds to the panel returning to its neutral state.

prior to the next consecutive maximum C_t, where irregularities are observed in C_t. Instances 4 and 5 corresponds to that of the convex panel at instance 1 ($t^\star = 0.91$) and instance 3 ($t^\star = 1.32$).

VII. CONCAVE PANEL WAKE AND FORCE PRODUCTION

The instantaneous thrust and side-force variations for the concave panel are presented in Figure 14. As for the square and convex panels, the maximum thrust coincides with local extrema in the side-force, and there are similar irregularities in the side-force at instances prior to maximum thrust. The wake structures at Instance 6 are shown in Figure 15. Instance 6 occurs immediately prior to the time of maximum thrust at $t^\star = 0.89$, and which corresponds to instance 1 for the convex panel and instance 4 for the square panel. At this instance, the concave panel is in an inward pitching motion (from a high-pitch state to the neutral state). The wake is dominated by vortex loops that are interconnected through a streamwise vortex rib (VR_1), which connects consecutive structures at their concave point. The detachment of TEV_6 is imminent as its legs distort toward the wake centerline. Compared to the other two panels, the wake distortion appears to be slower and less severe, and there is no evidence of the wake splitting. It appears that the lower thrust and efficiency of the concave panel is associated with its more compact and organized wake. The com-

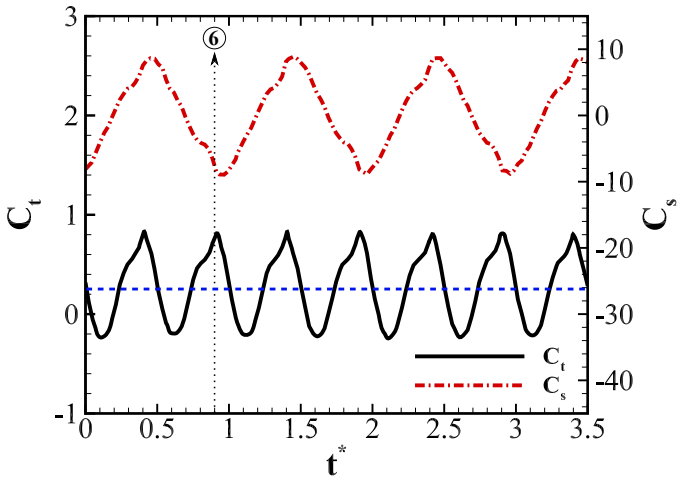

FIG. 14: Thrust (C_t) and side-force (C_s) coefficients for the concave panel. Instance 6 corresponds to moments after the panel's high-pitch orientation.

bination of these characteristics leads to a lower thrust and efficiency for concave panels. Furthermore, it is apparent that side-edge shear layers play a more important role in the formation and detachment of TEVs, which implies larger three-dimensional effects for the concave panel, and thus, lower thrust[17].

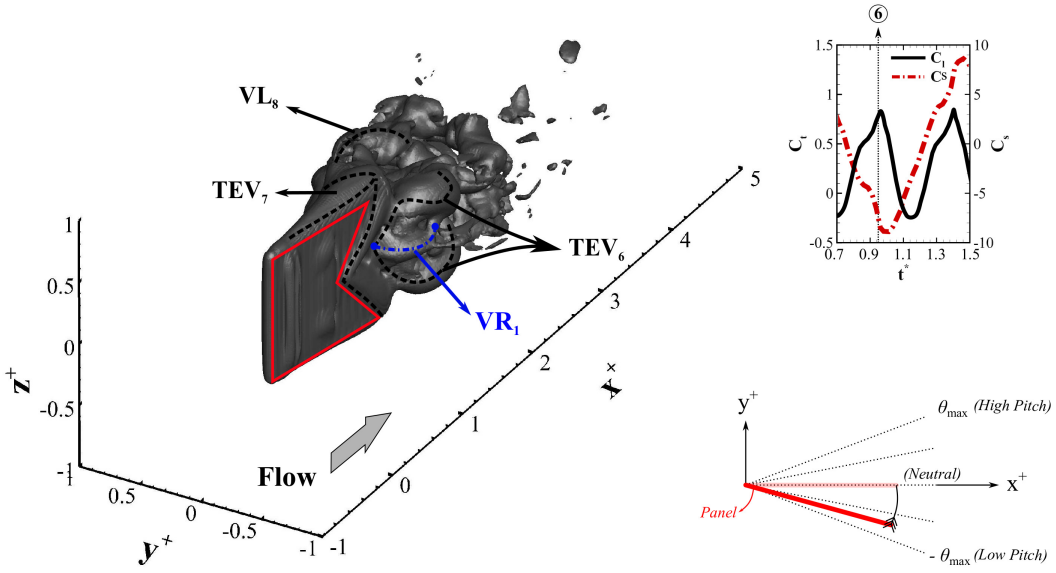

FIG. 15: Concave trailing edge panel at instance 6 ($t^\star = 0.89$). For symbols and notation see Figure 10.

VIII. CONVEX PANEL SURFACE PRESSURE

To connect the wake formation with the thrust more directly, we now examine the behavior the surface pressure. The pressure distributions are also of interest because in any application pressure is one of the few parameters that can be accessed as an input for an active control system.

The contours of pressure on the left and right faces of the convex panel are shown in Figure 16. At instance 1 (Figure 16a), the initial formation of LEV_1 is seen at the upstream boundary of a low pressure region LPA_1 on the right face of the panel (see also Figure 10). We have seen that TEV_1 remains attached to the panel shear layers on its upper and lower (side-) edges. This development imposes a high pressure region HPA_1 on the panel left face, corresponding to the growing TEV_1. Note that LPA_1 mirrors HPA_1 on the opposite face.

At instance 2, the merging of LEV_1 with the side-edge shear layers forms a distinct pressure signature on the panel right face, which is identified as C_2 in Figure 16b. The low pressure area LPA_2 is formed due to the on-going detachment of VL_2 (and formation of TEV_2) at instance 1 that remains in place during instance 2 (see Figures 10 and 11). However, there are relatively higher pressure zones (C_2 and B_2) formed within LPA_2 due to the merging of LEV_1 with side-edge shear layers and their subsequent wrapping around the trailing edge, which coincides with the stretching of TEV_2. In addition, this wrapping process somewhat mitigates the low pressure levels found near the trailing edge on the left face of the panel (A_2), where LEV_1 merges with the shear layers and feeds a newly forming TEV_2.

The pressure differences between the two faces of the panel increases in the regions near the side edges of the panel, which would strengthen the side-edge shear layers. At the same time, the integrated pressure difference between the two faces has decreased, corresponding to the decrease in thrust at this instance (Figure 11).

At instance 3, the surface pressure behavior on both faces of the panel (Figure 16c) follows the same trend as in the previous two instances, where the high pressure area HPA_3 on the panel right face corresponds to the development and detachment of TEV_2. The left face of the panel, where TEV_1 has transformed into the vortex loop VL_4, displays a low pressure region, LPA_3. The reversal of the high and low pressure regions on the right and left faces leads to a lower side-force generation, and thus switches the sign of the side-force slope.

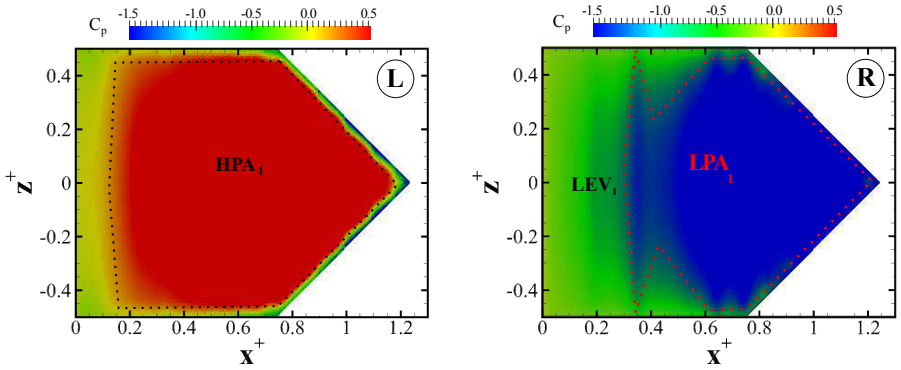

(a) Instance 1

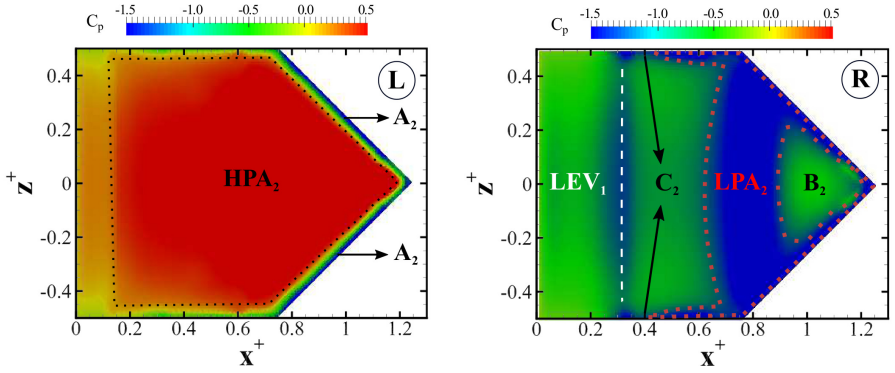

(b) Instance 2

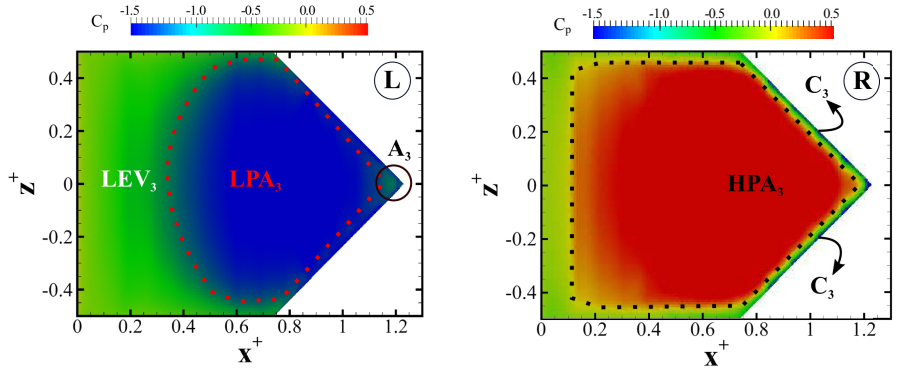

(c) Instance 3

FIG. 16: Contours of surface pressure on the left (**L**) and right (**R**) faces of the convex panel at (a) Instance 1, (b) Instance 2 and (c) Instance 3 (see Figures 10 and 12).

This phenomenon coincides with the reversal of the direction of pitching, which has been linked to a temporary reduction in thrust and the irregularities in C_t and C_s. In addition, the indications of a newly formed LEV_3 on surface pressure are evident at the upstream boundary of LPA_3.

IX. SQUARE PANEL SURFACE PRESSURE

The contours of surface pressure for the square panel are shown in Figure 17 at instances 4 and 5. At instance 4 (immediately after the time of maximum thrust), there exists a low pressure region, LPA_4, on the panel right face, which extends from $x^+ \approx 0.2$ to the panel trailing edge. The presence of this low pressure region corresponds to the imminent detachment of the TEV from the trailing edge, and its upstream boundary coincides with the presence of a LEV.

At instance 5 (just prior to the time of maximum thrust), there is a reversal of the low

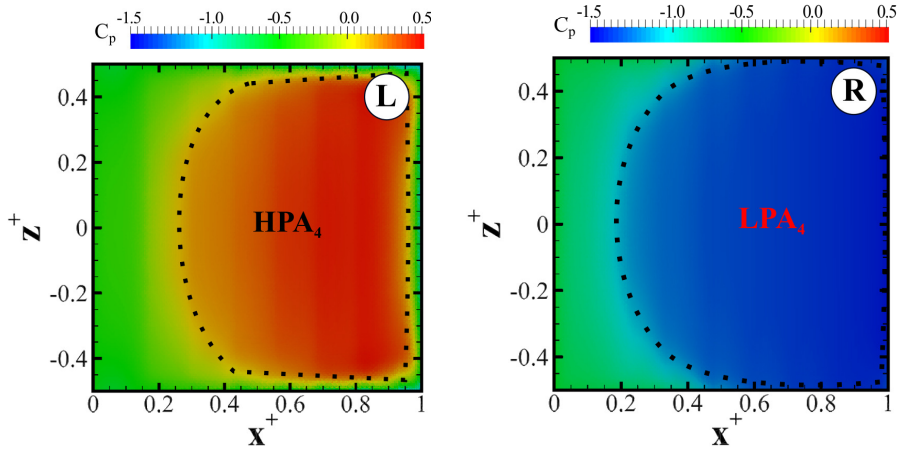

(a) Instance 4

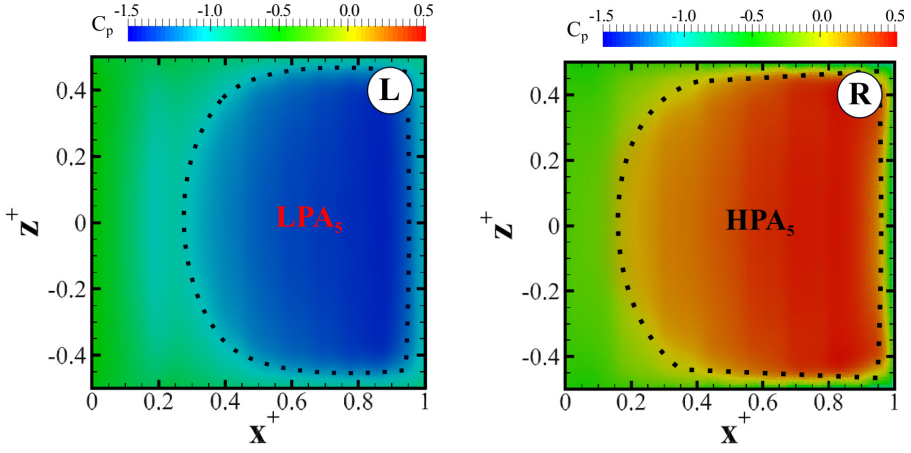

(b) Instance 5

FIG. 17: Contours of surface pressure on the left (**L**) and right (**R**) faces of the square panel at (a) Instance 4, and (b) Instance 5 (see Figure 13).

and high pressure regions on the panel faces, corresponding to the reversal in the direction of pitching motion, although the overall pressure difference between the two faces now appears to be a little smaller than that in instance 4. This may be an important observation, in that one could argue that vortex detachment occurs when the difference in pressure on opposite faces of the panel is a maximum. Intuitively, such a maximum would lead to local maximum or minimum in C_s, which agrees with the observations made in Section III. Since these maxima are associated with the detachment of TEVs, which in turn coincide with maximum in C_t, it is possible to establish a direct connection among wake events, force fluctuations and surface pressure variations. That is, TEV detachment from an oscillating panel leads to large streamwise pressure gradients across the panel faces, which produce extrema in C_s. Due to momentum transfer, the detachment of structures from the panel trailing edge (the formation of TEV) leads to a local maximum in C_t. Thus, the local maximum in thrust coincides with positive and negative extrema in side force.

As to the spanwise gradients, the presence of the side edges causes considerable curvature of the pressure contours, especially for $|z^+| > 0.3$. Nevertheless, the strongest effects of the side edges are confined to relatively narrow regions defined by $|z^+| > 0.42$ and $x^+ > 0.4$, which correspond to the regions where the side edge shear layers roll up

X. CONCAVE PANEL SURFACE PRESSURE

The behavior of the surface pressure on the faces of the concave panel is similar to that already reported for the convex and square panels (see Figure 18). The point of maximum

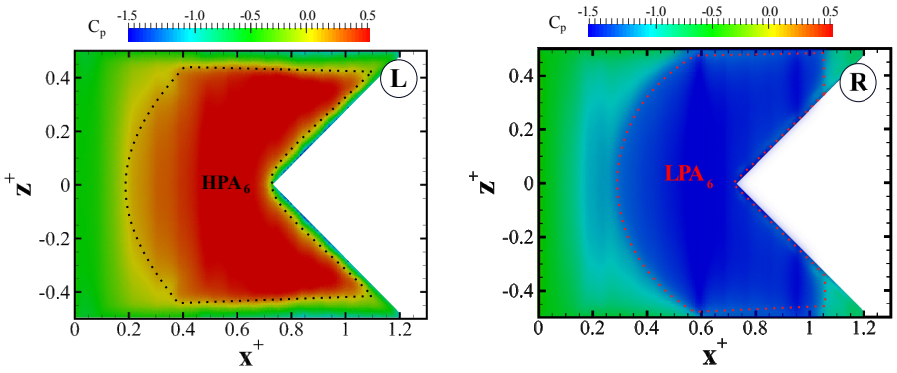

FIG. 18: Contours of surface pressure on the left (**L**) and right (**R**) faces of the concave panel at instance 6 (see Figures 14 and 15).

thrust at instance 6 coincides with minimum side force, which corresponds to the observation that the strength of the low pressure region (LPA_6) on the panel right face is larger than that of the high pressure region (HPA_6) on the left face. Also, the detachment of TEV_6 coincides with the presence of LPA_6 on the right face of the panel. Note that near the top and bottom tips of the panel, the pressure difference between the two faces of the panel is very small due to three-dimensional effects. Hence the tips contribute little to the thrust.

XI. DISCUSSION AND CONCLUSION

The experiments by Van Buren et al.[1] showed that the thrust produced by pitching panels, and their efficiency, increased as the trailing edge shape was changed from concave to square to convex. By examining the development of wake structures and their corresponding pressure distributions on the panel, we found that in all cases the maximum instantaneous thrust coincides with the detachment of a trailing edge vortex (TEV). In all cases, the leading edge vortex (LEV) eventually wraps around the trailing edge and merges with side-edge shear layers and connects to the legs of TEVs. This process leads to irregularities in the instantaneous thrust and side-force generated by the panel.

The shape of trailing edge has a strong effect on the wake development. In particular, as the LEV travels downstream on the panel, it moves away from the surface forming a vortex loop that remains attached to the surface by vortex "legs" that wrap around the sharp tips of the panel trailing edges to form TEVs that retain the shape of the trailing edge. The wakes are dominated by vortex loops with streamwise vortex legs that connect consecutive structures, and these loops retain the trailing edge angle (ϕ) in the immediate wake prior to their distortion downstream. The degree of distortion depends very much on the trailing edge angle, and it is weakest for the concave panel, where the wake width did not change substantially as it developed downstream ($x^+ \leq 3$). For the square and convex panels, however, the wake narrowed quickly and displayed highly distorted vortex legs and bent structures, which translates to larger pressure gradients on the panel surfaces and a larger mean thrust.

Our results suggest that by modifying the trailing edge shape beyond what was explored here, it may be possible to improve the performance further. In particular, for $\phi > 135^\circ$ it may be possible for the TEV to grow even larger before detaching and thereby further

increase the thrust for the same planform area. The larger thrust developed by the convex panel is partly explained by the observation that in the center-span of the panel, where the thrust generation is most important, the local Strouhal number is effectively higher because the local pitch amplitude is higher. In contrast, the concave panel has the longest chord at the top and bottom edges. Due to three-dimensional effects, the pressure differences between the two faces of the panel near the tips are small, and so the longer chord at the edges of the concave panel do not contribute much to the thrust.

The local surface pressure distributions on the panel faces also reflect the vortex formation and interaction processes in the immediate wake. Thus, the start of the leading edge vortex formation, the location of the vortices on the panel surface prior to detachment, and the TEV detachment, are identified with characteristic signatures in the surface pressure distribution. This connection may allow for the design of a control system to identify, track and modify the leading edge and trailing edge vortices in order to enhance the propulsive performance of simple propulsors.

ACKNOWLEDGMENTS

This study has received support from the National Science and Engineering Research Council of Canada (NSERC), and the U.S. Office of Naval Research under MURI grant number N00014-14-1-0533 (program director Dr. Robert Brizzolara). The authors are also grateful to Prof. Luigi Martinelli for his input on the grid quality discussion.

REFERENCES

[1]T. Van Buren, D. Floryan, D. Brunner, U. Şentürk, and Alexander J. Smits. Impact of trailing edge shape on the wake and propulsive performance of pitching panels. *Physical Review Fluids*, 2(1):014702, 2017.

[2]V. Sambiley. Interrelationships between swimming speed, caudal fin aspect ratio and body length of fishes. *Fishbyte*, 8:16–20, 1990.

[3]J. L. Sumich and J. F. Morrissey. *Introduction to the Biology of Marine Life*. Jones & Bartlett Learning, 2004.

[4]L. Guglielmini and P. Blondeaux. Propulsive efficiency of oscillating foils [j]. *European Journal of Mechanics B/Fluids*, 23:255–278, 2004.

[5]P. Blondeaux, F. Fornarelli, and L. Guglielmini. Numerical experiments on flapping foils mimicking fish-like locomotion. *Physics of Fluids*, 17(11):113601, 2005.

[6]J. H. J. Buchholz and A. J. Smits. On the evolution of the wake structure produced by a low-aspect-ratio pitching panel. *J. Fluid Mech.*, 546:433–443, 2006.

[7]R. T. Jantzen, K. Taira, K. O. Granlund, and M. V. Ol. Vortex dynamics around pitching plates. *Physics of Fluids*, 26(5):053606, 2014.

[8]M. S. Triantafyllou and G. S Triantafyllou. An efficient swimming machine. *Scientific American*, 272(3):64–71, 1995.

[9]J. H. J. Buchholz and A. J. Smits. Wake of a low aspect ratio pitching plate. *Physics of Fluids*, 17(9):091102, 2005.

[10]J. H. J. Buchholz and A. J. Smits. The wake structure and thrust performance of a rigid low-aspect-ratio pitching panel. *J. Fluid Mech.*, 603:331–365, 2008.

[11]M. A. Green, C. W. Rowley, and A. J. Smits. The unsteady three-dimensional wake produced by a trapezoidal pitching panel. *J. Fluid Mech.*, 685:117–145, 2011.

[12]J. T. King, R. Kumar, and M. A. Green. Experimental observations of the three-dimensional wake structures and dynamics generated by a rigid, bioinspired pitching panel. *Physical Review Fluids*, 3(3):034701, 2018.

[13]G. V. Lauder. Function of the caudal fin during locomotion in fishes: Kinematics, flow visualization, and evolutionary patterns. *American Zoologist*, 40(1):101–122, 2000.

[14]M. G. Chopra. Hydromechanics of lunate-tail swimming propulsion. *J. Fluid Mech.*, 64(2):375–392, 1974.

[15]G. Karpouzian, G. Spedding, and H. K. Cheng. Lunate-tail swimming propulsion. part 2. performance analysis. *J. Fluid Mech.*, 210:329–351, 1990.

[16]G. Liu and H. Dong. Effects of tail geometries on the performance and wake pattern in flapping propulsion. In *ASME 2016 Fluids Engineering Division Summer Meeting*, page V01BT30A002. American Society of Mechanical Engineers, 2016.

[17]M. A. Green and A. J. Smits. Effects of three-dimensionality on thrust production by a pitching panel. *J. Fluid Mech.*, 615:211–220, 2008.

[18]M. C. Leftwich and A. J. Smits. Thrust production by a mechanical swimming lamprey. *Experiments in Fluids*, 50(5):1349–1355, 2011.

[19]A. Hemmati, D. H. Wood, and R. J. Martinuzzi. Wake dynamics behind a normal thin flat plate at moderate reynolds numbers. In *Progress in Turbulence VI*, pages 265–269. Springer International Publishing, 2016.

[20]A. Hemmati. *Evolution of large-scale structure in the wake of sharp-edge thin flat bodies*. PhD thesis, University of Calgary, Calgary, AB, Canada, 2016.

[21]U. Şentürk and A. J. Smits. Numerical simulations of the flow around a square pitching panel. *Journal of Fluids and Structures*, 76:454–468, 2018.

[22]U. Şentürk, D. Brunner, H. Jasak, N. Herzog, C. W. Rowley, and A. J. Smits. Benchmark simulations of flow past rigid bodies using an open-source, sharp interface immersed boundary method. *Progress in Computational Fluid Dynamics*, 2018.

[23]D. Brunner. Performance and wake structures of efficient fish. Master's thesis, Zurich University of Applied Sciences, Zurich, Switzerland, 2016.

[24]K. Taira and T. Colonius. Three-dimensional flows around low-aspect-ratio flat-plate wings at low Reynolds numbers. *J. Fluid Mech.*, 623:187–207, 2009.

[25]V. D. Narasimhamurthy and H. I. Andersson. Numerical simulation of the turbulent wake behind a normal flat plate. *International Journal of Heat and Fluid Flow*, 30(6):1037–1043, 2009.

[26]J. Jeong and F. Hussain. On the identification of a vortex. *J. Fluid Mech.*, 285:69–94, 1995.